ASCE

Reliability Evaluation Based on Multiple Response Surfaces Method Considering Construction Uncertainties of Cable Tension for a Hybrid Roof Structure

Youbao Jiang, M.ASCE[1]; Hao Zhou[2]; Lei Wang, M.ASCE[3]; Zhao Chen[4]; Teng Tang, Ph.D.[5]; and Sondipon Adhikari[6]

Abstract: For large-span hybrid roof structures, the construction uncertainties of cable tension usually have significant influences on the roof's mechanical performance and should be considered in reliability evaluation. An effective approach to quantify uncertainties of cable tensions and evaluate structural reliability is proposed to carry out the studies by combining finite-element simulation with the multiple response surfaces method. Taking a hybrid roof structure with cables and steel trusses as an example, the main procedures on this issue are illustrated. First, a finite-element model is established for the hybrid roof structure considering construction deviations, such as the deviations of cable force between the design values and the real measured values. The ultimate bearing capacity of the structure is calculated for models with and without deviations, and the effects of construction deviations on structural bearing capacity are analyzed. Then, an uncertainty model of cable tension for structural reliability evaluation is proposed by establishing the statistics of initial strain in a structural analysis based on the monitored deviations. With subspace division and limit state sample (or sample pair), the multiple response surfaces method is developed to solve reliability for examples with complex failure functions. It is found that the hybrid roof structure has a high reliability index about 6.76; and the uncertainties of cable tensions have a large impact on the reliability, especially the uncertainties of the upper suspension cable tensions and the back cable tensions. **DOI: 10.1061/AJRUA6.0001152.**

Author keywords: Hybrid roof structure; Cable; Steel truss; Multiple response surfaces method; Reliability; Uncertainty of cable tension; Construction deviation.

Introduction

In recent years, large-span space structures (e.g., cable domes, shell structures) have been widely used in public buildings, such as stadiums and airports, due to their good mechanical performance and light self-weight (Morino 1998; Phocas and Alexandrou. 2018; Yan et al. 2019; Wakefield 1999).

To be largely different from simple frame structures in mechanical performance, the large-span space structures often have various structural types, e.g., foldable kirigami structure (Cai et al. 2019b; Zhang et al. 2020), and need complex analysis and design techniques. In order to better promote the development of large-span space structures, several scholars have carried out a significant amount of research on tensegrity structures, which can theoretically be constructed with the largest span. Fuller (1975) first studied this novel structure. However, this tensegrity dome structure has not been perfectly used in engineering practice. Based on Fuller's thinking, Geiger et al. (1986) studied a new structure called cable dome and successfully implemented it in the circle roof structure of the stadium for gymnastics and fencing games of the Seoul Olympic Games in 1986. In addition, further mechanical analyses of the tensegrity structures have been carried out. For example, Kebiche et al. (1999) discussed the geometric nonlinearity of tensegrity structures. Sultan et al. (2001, 2002) studied the linear dynamics of tensegrity structures and derived their linear motion equation with arbitrary equilibrium configuration, and also investigated prestressing problems of tensegrity structures. Williamson et al. (2003) studied the requirement of initial equilibrium state of tensegrity structures. Feng (2005) carried out a comprehensive study on the structural behaviors of tensegrity domes, and performed a prototype analysis of the first tensegrity dome—the Georgia Dome—with numerical calculations. Cai et al. (2019a) investigated the effects of initial imperfections of struts on the mechanical behavior of tensegrity structures.

By comparison, hybrid structures, consisting of cables and rigid structures (e.g., shell structure, arch structure, truss structure), have attracted more attention due to the convenience of construction. Yasuhiko and Wu (1999) proposed a structural behavior analysis method and made model tests of the hybrid structures considering the effects of both prestressing and static load deformation. Jiang et al. (2016) proposed an effective method to study the stiffness of inner concave cable-arch structures based on the force method,

[1]Professor, School of Civil Engineering, Changsha Univ. of Science and Technology, Changsha 410114, China. Email: youbaojiang@csust.edu.cn

[2]Doctoral Student, School of Civil Engineering, Changsha Univ. of Science and Technology, Changsha 410114, China. Email: haozhou@stu.csust.edu.cn

[3]Professor, School of Civil Engineering, Changsha Univ. of Science and Technology, Changsha 410114, China (corresponding author). Email: leiwang@csust.edu.cn

[4]Master, School of Civil Engineering, Changsha Univ. of Science and Technology, Changsha 410114, China. Email: 470319517@qq.com

[5]YueYang SanHe Investment Management of Airport Construction Co. Ltd., Airport Ave., Airport New Village, Yueyang 414000, China. Email: tang7889@163.com

[6]Professor, College of Engineering, Swansea Univ., Swansea SA1 8EN, UK. Email: s.adhikari@swansea.ac.uk

Note. This manuscript was submitted on September 18, 2020; approved on March 31, 2021; published online on June 22, 2021. Discussion period open until November 22, 2021; separate discussions must be submitted for individual papers. This paper is part of the ***ASCE-ASME Journal of Risk and Uncertainty in Engineering Systems, Part A: Civil Engineering***, © ASCE, ISSN 2376-7642.

which has the main advantage of the ratio of each deformation (such as bending deformation) to the total deformation be clearly obtainable through a simplified analysis.

For both tensegrity structures and hybrid structures, which include flexible cable members, the nonlinear effect is obvious. Therefore, the form-finding analysis is important for the design and construction of structures. Tibert and Pellegrino (2003) as well as Juan and Tur (2008) summarized the current form-finding methods for tensegrity structures. Cai and Feng (2015) proposed an effective numerical form-finding method for regular and nonregular tensegrity structures. Zhang and Ohsaki (2006) presented an improved numerical method for finding the form of tensegrity structures that can automatically adjust the values of the force densities to adapt to the requirement on rank deficiency.

As is well known, the node deviations in construction have a great impact on the structural performance. Therefore, more attention has been paid to evaluating the effects of construction deviations on structures. For example, aiming at the tension system of the crescent-shaped Yueqing Stadium in China, Deng et al. (2013, 2016) studied the effects of cable pretension deviations on structural mechanics, which is caused by the geometric deviations (e.g., manufacturing error of component length and installation error of anchor joint). However, a deterministic analysis is mainly involved, and quantifying the influences of construction deviation uncertainties on structural reliability needs to be further carried out.

At present, reliability-based design and evaluation has been widely applied in engineering practice. Many methods are proposed for reliability calculation of practical structures, which are usually with implicit performance functions. Among them, the surrogate model method is able to obtain relatively accurate results with a small number of samples (Dubourg et al. 2013), and it is widely accepted in the field of reliability analysis. It approximates the performance function to calculate the failure probability by constructing a surrogate model. The commonly used surrogate model methods include the kriging model (Xue et al. 2017), polynomial chaos expansion (PCE) (Marelli and Sudret 2018), artificial neural networks (ANNs) (Papadopoulos et al. 2012), and response surface method (RSM) (Jiang et al. 2015). Among these, the kriging model usually has good performance in approximating local characteristics. Based on this characteristic, scholars have proposed many adaptive kriging methods (Teixeira et al. 2020; Wang and Shafieezadeh 2019; Xiao et al. 2020) for structural reliability analysis. However, the construction of the kriging model is relatively complex, and it is very time-consuming to construct a kriging model in the case of large samples. In addition, the fitting effect of the kriging model is not good for high-dimensional problems. The PCE model has good performance in approximating global characteristics, but it has the phenomenon of dimension curse, that is, with the increase of the dimension of input variables, the computation task needed for model construction increases significantly (Schobi et al. 2015). Therefore, many scholars have proposed the corresponding sparse method to overcome the dimension curse phenomenon.

RSM has three main forms: using polynomial-basis functions, radial-basis functions, and spline-basis functions (Teixeira et al. 2020). Due to the compromise between practicability and efficiency, polynomial-basis RSM is one of the most popular metamodeling techniques for reliability (Guimarães et al. 2018), and many scholars have studied and developed it. Ju et al. (2013) proposed an adaptive response surface method based on the moving least-squares method. Jiang et al. (2015, 2017) proposed an efficient response surface method based on techniques of generation of a uniform support vector, which has the advantages that it can dramatically increase the proportion of support vectors to the whole sample and requires fewer samples in function fitting. Hadidi et al. (2017) proposed another efficient response surface method, which can greatly reduce the number of samples by using an exponential response surface model and an experimental updating technique. Moreover, the accuracy of the proposed method is improved by judiciously selecting the location of sample points that are close to the actual limit state surface. Examples show high efficiency of this method for reliability analysis of simple structures, e.g., planar truss or planar frame. However, the conventional response surface methodology has some shortcomings in reliability analysis, especially for structures with complex and high-dimensional failure functions, and it is also affected by the phenomenon of dimension curse (Guimarães et al. 2018).

For large hybrid roof structures (HRSs) with complex mechanical behaviors and a lot of uncertainties, it is difficult to quantify the influences of these uncertainties on structural safety. In order to solve these problems, this paper establishes an uncertainty model of cable force for the finite-element structure with the measured construction deviation and proposes a reliability method based on the multiresponse surface technology. Combining the uncertainty model with the reliability method, the reliability index of the structural bearing capacity is calculated. The influence of different cables on the reliability of the structure is also discussed.

Structural Bearing Capacity Analysis

Introduction of Hybrid Roof Structure

A terminal building is selected, which is in Yueyang City, China, and has a long-span hybrid roof structure. The whole structure consists of three parts: steel trusses, cables, and membranes, as shown in Figs. 1 and 2. Because the membranes are supported by the steel trusses and cables and used for exterior protected usage only, the steel trusses and cables are considered only in the following bearing capacity analysis, as shown in Fig. 3. The truss structures are used for both main bearing trusses in the middle and towers in the sides.

It is seen that the steel trusses include truss beam (TB), truss column (TC), truss tower (TT), truss support (TS), and steel column (SC). The cables include upper suspension cables (C_U), lower suspension cables (C_L), back cables in east and west sides (C_E and C_W), membrane-supported cables (C_S), boundary cable (C_B), and

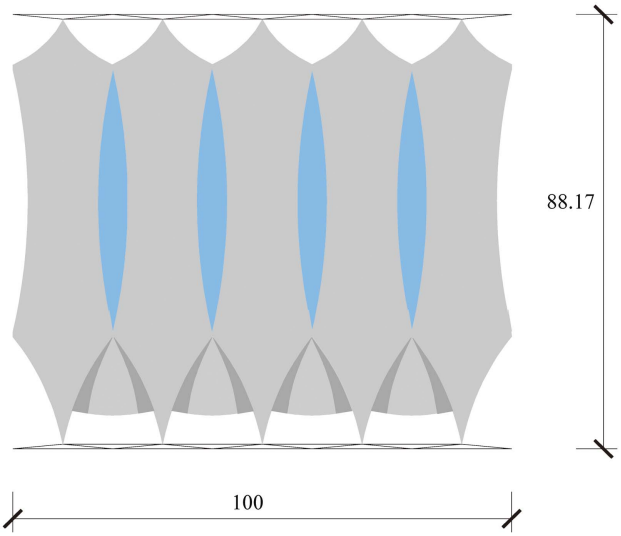

Fig. 1. Plan view of terminal building (unit: meters).

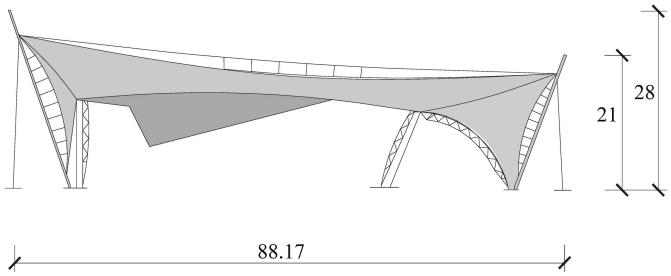

Fig. 2. Elevation view of terminal building (unit: meters).

pendent cable (C_P). The nominal strength of cables and steel trusses are 1,670 and 345 MPa, respectively, and other design information is listed in Tables 1 and 2.

Design Model without Deviations

Based on the preceding section information and structural layout, the finite-element model of the HRS was established using ANSYS 12.0 software, as shown in Fig. 4, where the Link10 tension element is used for cables and Beam188 element is used for steel members. There are 9,359 nodes and 5,390 elements in the finite-element model.

In the finite-element model, the structural parameters of cables, e.g., pretensions and strength, are assumed to adopt their design values, as given in Table 1.

Structural Model with Deviations

Because the cables often play an important role in the hybrid roof structure, their tensions should be monitored carefully during construction. To match well with their design values, key cables are monitored in construction, as shown in Fig. 5. The process of tensioning the suspension cables is shown in Fig. 6.

It is known that the measured cable tensions vary in the construction steps. After the construction of all cables and trusses is finished, the measured cable tensions and their design tensions as well as the errors are compared. The results are given in Table 3, where T_d and T_m denote their design value and measured value, respectively.

It is seen that the largest error is about 20% for the C_{L1} cable. Based on the measured cable tensions, the finite-element model can be updated, and the structural model with deviations are obtained for capacity analysis.

Comparisons of Ultimate Bearing Capacity of Two Models

When the initial prestress is applied to the cable and the ultimate bearing capacity analysis of the structure, the shape of the structure will change greatly, and the small deformation assumption will no longer be applicable. In order to improve the calculation accuracy, considering the material and geometric nonlinearity, the ultimate bearing capacity of the two models is analyzed. Considering the unfavorable design load combination, the ultimate bearing capacity can be calculated at 1.2DL + 1.4SL + 0.98LL, where DL, SL, and LL represent dead load, snow load, and live load, respectively, at a temperature drop of 24°C [GB50009-2012 (MOHURD 2012)].

For the structural model without cable tension deviations, the maximum vertical displacement is about 1.12 m when the structure reaches the ultimate limit state (e.g., the maximum bearing capacity or excessive deformation which may cause structural collapse), which occurs at Node 141 of the upper suspension cable in the middle of the structure, as shown in Fig. 7. However, for the structural model with cable tension deviations, Node 190 has the maximum displacement when the structure is at ultimate limit state. The load–displacement curves of Nodes 141 and 190 are shown in Fig. 8. From the nonlinear curves, it can be seen that the structural nonlinear behaviors are strong. The ultimate bearing capacity of the design model and the measured model are 2.21 and 2.22, respectively, and there is little difference between them. However, the difference of ultimate deformation is large—1.12 and 1.29 m, respectively—and the deformation increases by 15.2%. The results show that the cable force deviation has little influence on the bearing capacity of the structure, but has a great influence on the displacement of the structure under the limit state, which cannot be ignored. The maximum tensile stress of the cable is 457 MPa, which is far less than the design strength of 1,670 MPa. The failures of the steel structure dominate the failures of the structure in structural bearing capacity analysis.

Uncertainty Model of Cable Tension Forces

As mentioned previously, the actual cable tensions are measured after construction is finished. For some cables, the measured tensions get larger than their design value, while for other cables

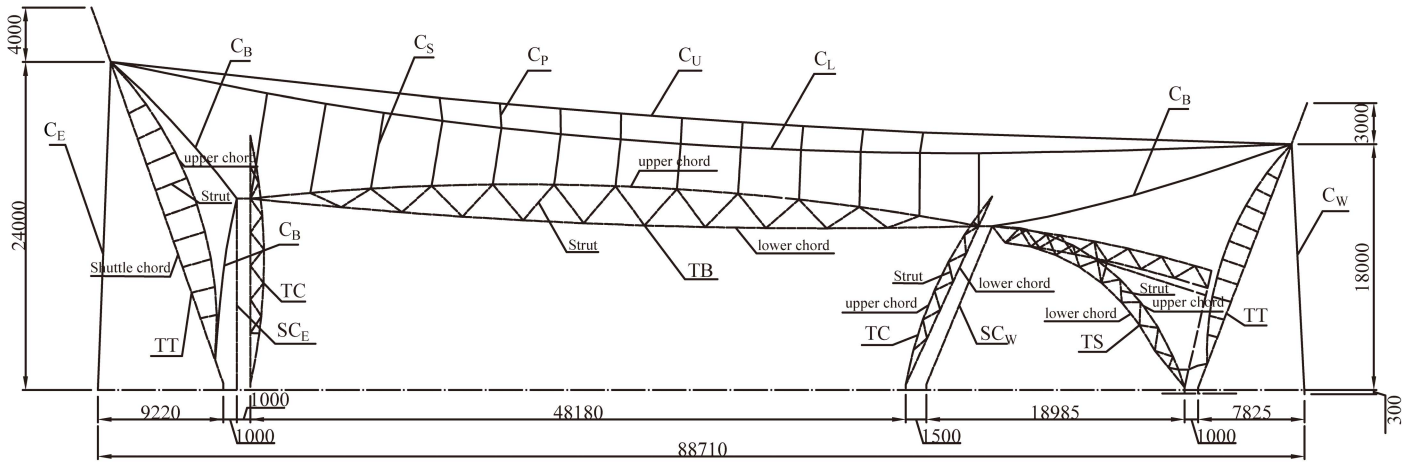

Fig. 3. Configurations of roof structure.

ASCE-ASME J. Risk Uncertainty Eng. Syst., Part A: Civ. Eng., 2021, 7(3): 04021033

Table 1. Design information of cable structure

Member name	D_w (mm)	N_w	Pretension (kN)
C_E	140	10	3,915
C_W	140	10	4,040
C_U	100	5	1,000
C_L	120	5	2,000
C_S	20	130	20
C_B	30	10	80
C_P	20	45	0.1

Note: D_w and N_w = diameter and number of cables, respectively.

Table 2. Design information of steel structure

Member name	Position	Member section
TB	Upper chord	650 × 20
	Struts	426 × 12
	Lower chord	180 × 8
TC	Upper chord	325 × 12
	Struts	140 × 6
	Lower chord	325 × 10
SC	West side	500 × 16
	East side	650 × 16
TS	Upper chord	325 × 10
	Struts	140 × 6
	Lower chord	219 × 10
TT	Shuttle chord	850–1,309 × 24–36
	Struts	140 × 6
	Lower chord	245 × 10

Note: Cross section of member: (diameter) × (thickness).

the measured tensions get smaller. However, due to uncertainties in service, e.g., creep of cable and rheologic changes, which may cause the prestress loss of cables (Dai et al. 2020; Kmet and Mojdis 2013; Kmet et al. 2007), and possible damage under long-time actions (Wang et al. 2019), the cable tensions would present complex changes by mechanical interactions and thus become uncertain during the service period. Not carefully considering the uncertainties may lead to an overestimation of safety or even an erroneous judgment. The whole structure failing will cause huge losses.

For the finite-element model of structure, the pretension of cable is simulated by setting initial strain in the Link 10 element. In order to consider the uncertainties of cable tensions practically, the initial strain of the corresponding cable can be multiplied by an uncertainty factor γ in the finite-element model. It is well known that the uncertain variables such as material properties, geometric parameters, and dead loads of the structure will fluctuate around the mean values rather than around the nominal values (Cheng 2010). Moreover, based on 30 sets of tension error data in Table 3, the mean value of deviations between design tension and measured tension is calculated as about 0, indicating that the uncertainty factor γ can reasonably be considered as 1.0. Therefore, the mean value of the uncertainty factor γ is considered as 1.0. The possible maximum variation of cable tension is assumed to be 20%, which matches well with the maximum error between the actual tension and the designed tension in Table 3. Following this assumption, the standard deviation of the uncertainty factor γ corresponding to the initial strain can be determined. For example, structural analysis shows that if the cable force of the upper suspension cable C_U needs to be increased by 20% from 1,080 to 1,300 kN, the corresponding initial strain should be increased by 30%, that is, the initial strain factor γ_1 should be 1.3, as listed in Table 4, which is the simulated design tension in the finite-element model (with a small difference

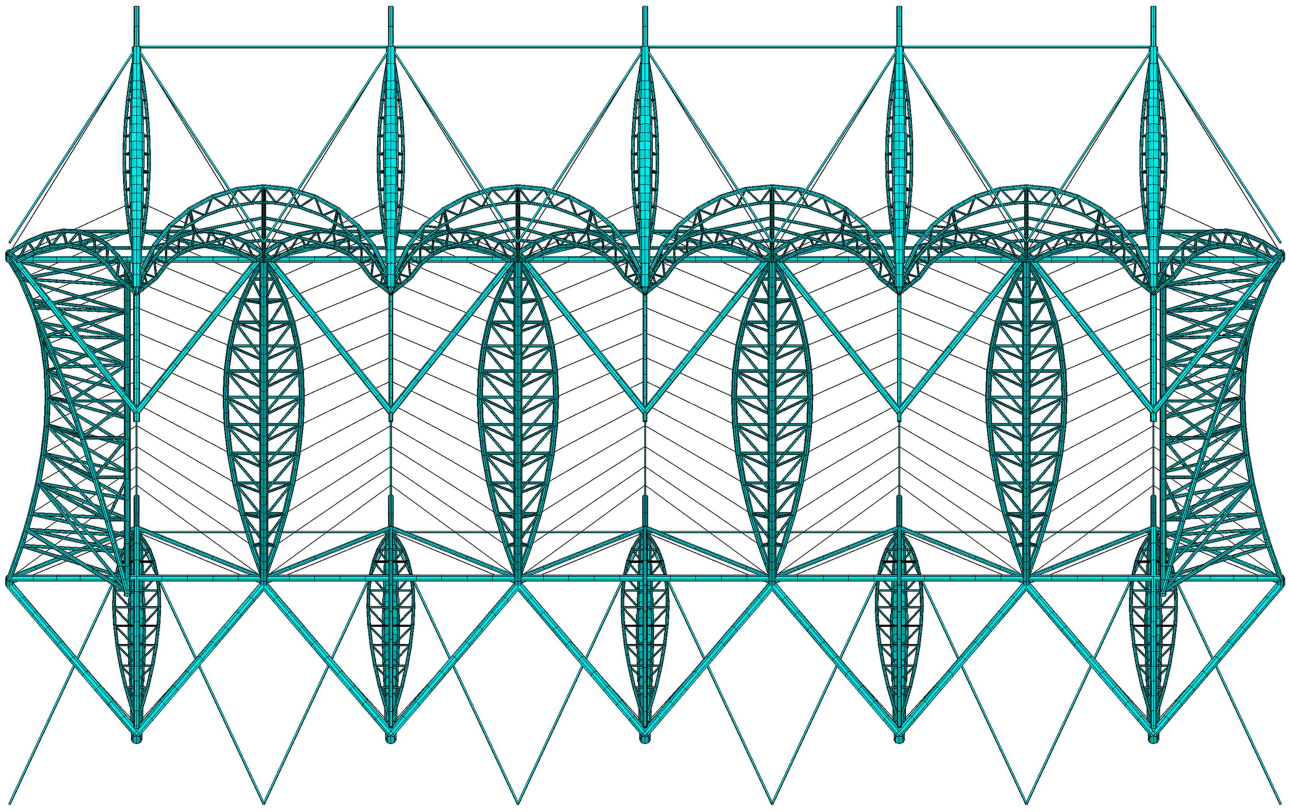

Fig. 4. Finite-element model of the HRS.

ASCE-ASME J. Risk Uncertainty Eng. Syst., Part A: Civ. Eng., 2021, 7(3): 04021033

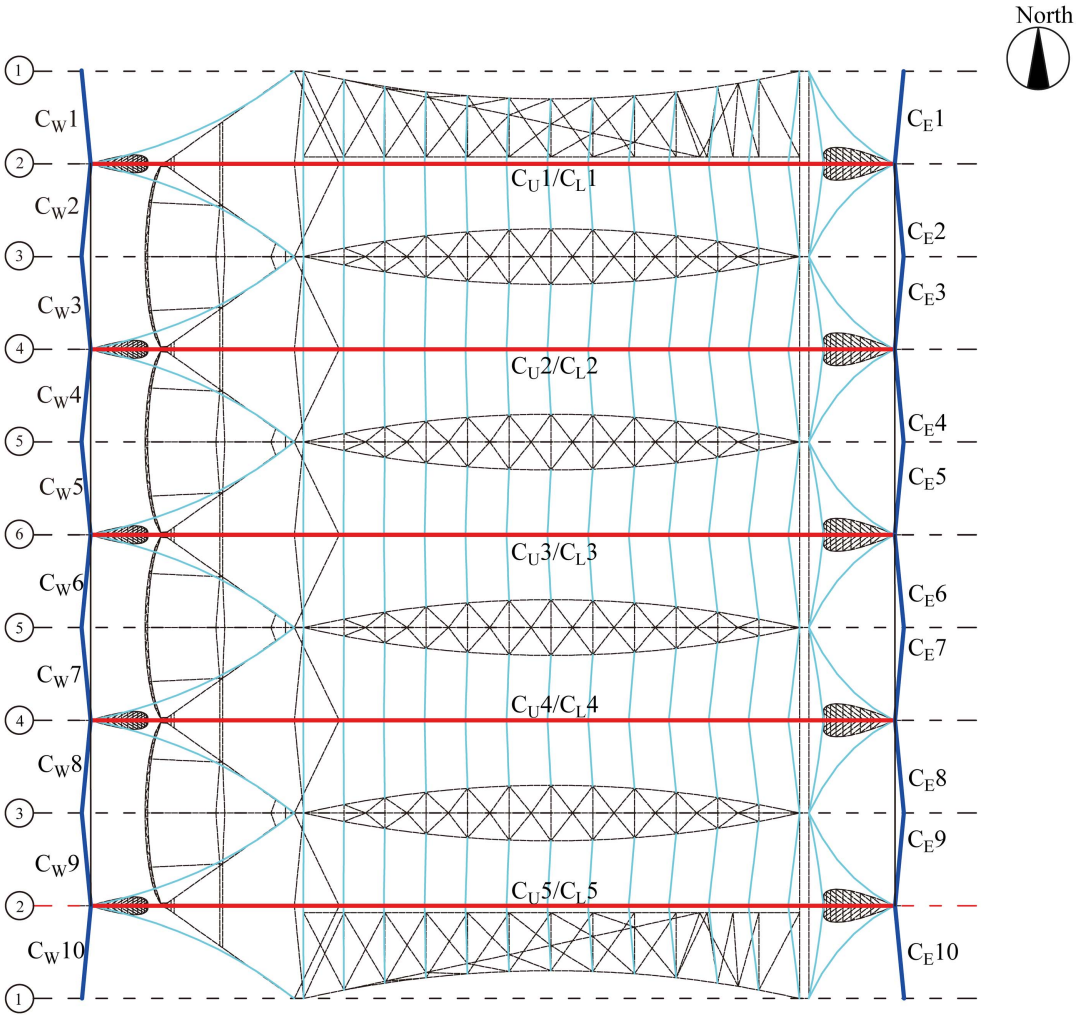

Fig. 5. Locations of monitored cables.

Fig. 6. Tensioning the suspension cables.

from the real design tension of 1,000 kN due to simulation errors). Let T_{pre} and T_{post} be the cable force value before and after adjusting initial strain, respectively. The error v between them is given by

$$\nu = \frac{T_{post}|_{\varepsilon_i' = \gamma_i \varepsilon_i} - T_{pre}}{T_{pre}}, \quad i = 1, 2, 3, 4 \tag{1}$$

where ε_i = initial strain.

Table 3. Designed and measured pretensions of each cable

Cable	T_m (kN)	T_d (kN)	Error (%)
C_U1	966	1,000	−3.4
C_U2	913	1,000	−8.7
C_U3	875	1,000	−12.5
C_U4	923	1,000	−7.7
C_U5	944	1,000	−5.6
C_L1	2,431	2,000	21.6
C_L2	2,267	2,000	13.4
C_L3	2,236	2,000	11.8
C_L4	2,244	2,000	12.2
C_L5	2,311	2,000	15.6
C_W1	4,306	4,040	6.18
C_W2	3,716	4,040	−8.72
C_W3	4,126	4,040	2.08
C_W4	3,654	4,040	−10.56
C_W5	3,289	4,040	−22.83
C_W6	3,423	4,040	−18.03
C_W7	3,834	4,040	−5.37
C_W8	3,953	4,040	−2.20
C_W9	3,887	4,040	−3.94
C_W10	4,229	4,040	4.47
C_E1	4,075	3,915	3.93
C_E2	3,950	3,915	0.89
C_E3	3,706	3,915	−5.64
C_E4	3,734	3,915	−4.85
C_E5	3,484	3,915	−12.37
C_E6	3,091	3,915	−20.06
C_E7	3,667	3,915	−6.76
C_E8	3,747	3,915	−4.48
C_E9	3,704	3,915	−5.70
C_E10	4,066	3,915	3.71

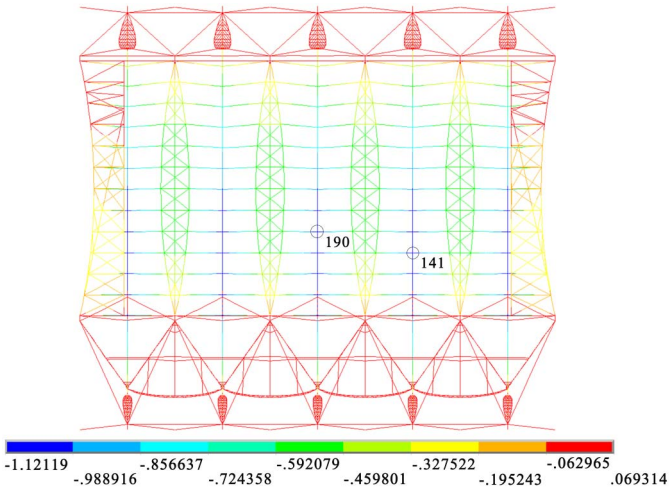

Fig. 7. Displacement distributions in limit state.

If the cable tension deviation is assumed to follow a normal distribution (Cheng 2014; Cheng 2010) and the maximum varying range is considered as $[\mu - 2\sigma, \mu + 2\sigma]$ (μ = mean value, σ = standard deviation) with 95.5% confidence probability, then the adjustment of initial strain leading to a variation of cable tension by 20% can be assumed as 2σ (two times the standard deviation). For example, for the upper suspension cable C_U, the standard deviation of the initial strain factor can be determined as 0.15, and the mean value is 1.0 as mentioned previously. Similarly, structural analysis results show that for other cables, the initial strain factor should be adjusted to $\gamma_2 = 1.4$, $\gamma_3 = 1.5$, and $\gamma_4 = 1.5$, respectively, if the cable force T_{post} is increased by about 20%. To summarize, the required initial strain factors of cables and the corresponding increases of tensions are listed in Table 5.

Based on the data, the statistics for uncertainties of cable tension are obtained and given in Table 6. They are used for the following reliability evaluations.

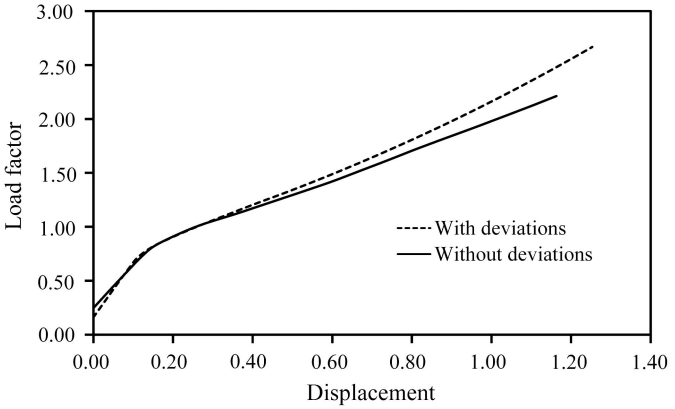

Fig. 8. Comparisons of ultimate bearing capacity of two models.

Table 4. Variations of cable tensions with increase of cable C_U tension by 30%

Cable	T_{post} (kN)	T_{pre} (kN)	v (%)
C_U	1,300	1,080	**20.25**
C_L	1,860	1,990	−6.67
C_E	4,170	4,060	2.76
C_W	4,450	4,350	2.24

Note: The quoted value in the text is highlighted in bold font.

Table 5. Initial strain factors and the increases of tensions

Initial strain factor	Cable	T_{post} (kN)	T_{pre} (kN)	v (%)
$\gamma_1 = 1.3$	C_U	1,300	1,080	20.25
$\gamma_2 = 1.4$	C_L	2,430	1,990	22.16
$\gamma_3 = 1.5$	C_E	4,970	4,060	22.46
$\gamma_4 = 1.5$	C_W	5,320	4,350	22.14

Table 6. Statistics for uncertainties of cable tension

Variable	Distribution	μ	σ
γ_1	Normal	1.0	0.15
γ_2	Normal	1.0	0.20
γ_3	Normal	1.0	0.25
γ_4	Normal	1.0	0.25

Reliability Method Based on Multiple Response Surfaces Techniques

Multiple Response Surfaces for Function Fitting

As mentioned previously, the conventional response surface methods often use samples not on the limit state surface, and select a single response surface model to carry out function fitting for

reliability analysis of large complex structures, which possibly causes inaccurate function fitting results. Therefore, this paper develops the limit state samples and multiple response surfaces (MRSs) based on subspace division techniques to carry out function fitting.

Generally, both the number and distributions of sample points are important factors affecting the function fitting accuracy. To obtain a uniform distribution of samples, the uniform design is applied widely with a uniform design table. The samples produced by the uniform design method are relatively independent and uniform, compared with those produced by other methods. Therefore, the uniform design method is suitable to be used to generate initial sample points for acquisition of limit state samples. If the random variables are given, the uniform design is carried out by selecting a uniform table $U_n(q^m)$ first, where n is the number of experiments, m is the maximum number of variables, and q is the number of levels of each variable (Fang and Wang 1994). A random variable in physical space can be transformed into a standard normal variable by the Rosenblatt transformation (Rosenblatt 1952). Herein, to simplify the introduction of failure function fitting, we start with the assumption that all random variables are standard normal variables. The initial uniform samples in the standard normal space are obtained according to Eq. (2)

$$x_{ij} = \left[\frac{2(u_{ij}-1)}{q-1} - 1\right]\lambda \tag{2}$$

where u_{ij} = element of the selected uniform table; x_{ij} = corresponding element in the standard normal space; and λ = parameter for the possible distribution range of samples and is generally taken as 3.0, and the corresponding confidence probability is 99.7%. Then use Eq. (3) to transform all initial uniform samples in the standard normal space X into those in the actual space Y

$$Y_i = F_{Y_i}^{-1}[\Phi(X_i)] \tag{3}$$

where $F_{Y_i}^{-1}()$ and $\Phi(\cdot)$ are the inverse function of the cumulative distribution function of variable Y_i and the cumulative distribution function of the standard normal variable X_i, respectively. With the sample points in the Y-space, the finite-element model is built and a deterministic structural failure analysis is carried out, and the ultimate load $F_{\lim}$ is obtained. Then combine the ultimate load with other resistance variables to obtain a limit state samples in the Y-space. Finally, the limit state samples in the X-space are obtained with Eq. (4)

$$X_i = \Phi^{-1}[F_{Y_i}(Y_i)] \tag{4}$$

Due to complex structural properties, the real limit state surface is also quite complex. For this reason, the whole limit state surfaces can be divided into multiple subsurfaces to obtain an accurate approximation. As is well known, the closer the point on the limit state surface is to the origin in the standard normal space, the greater the influence on the failure probability. Therefore, it is necessary to pay attention to the point closest to the origin. If X_0 is assumed as the closest sample point to the origin among all sample points, then an inner product coefficient of X_0 and X_i is calculated by Eq. (5), and the total space can be divided into multiple subspaces for function fitting according to the values of this coefficient

$$\rho_0(i) = (X_0 \cdot X_i)/\|X_0\|/\|X_i\| \quad i = 1, 2, \ldots, N \tag{5}$$

where N = number of the sample points.

The quadratic polynomial without cross terms is usually selected to consider the nonlinear characteristics of the complex failure function for function fitting. If limit state sample points are used, then it is expressed as

$$\bar{g}(X) = a + \sum_{i=1}^{m} b_i X_i + \sum_{i=1}^{m} c_i {X_i}^2 = 0 \quad i = 1, 2, \ldots, m \tag{6}$$

where a, b_i, and c_i = fitting coefficients; m = number of variables; and a can be taken as 1.0 for limit state sample points.

For all sample points, sort the values of $\rho_0(i)$, and select s representative values to divide the inner product coefficient into s ranges $[\rho_0(l), \rho_0(l-1)]$ $(l = 1, 2, \ldots, s)$, which satisfy that $1 = \rho_0(1) \geq \rho_0(2) \geq \rho_0(3) \geq \cdots \geq \rho_0(s)$. Within any range, the corresponding number of sample points is selected as $2m$ to satisfy that the fitting coefficients can be determined properly. Then the whole space can be divided into s subspaces: $\Omega_1, \ldots, \Omega_s$, as shown in Fig. 9, The response surface fitting is carried out in each subspace, and s response surfaces are obtained.

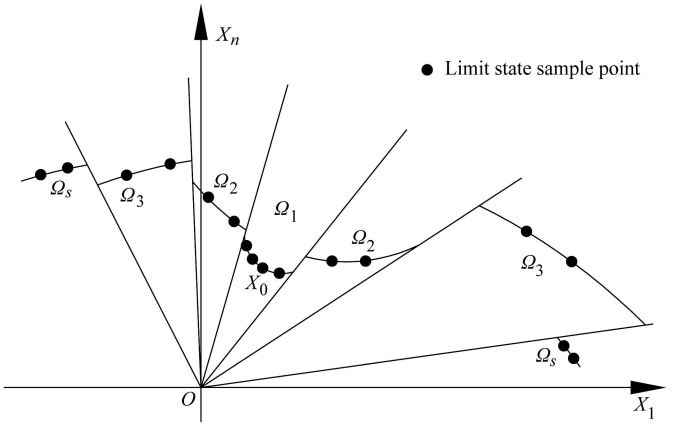

Fig. 9. Subspace divisions for multiple response surfaces.

To combine with support vector machine techniques in function fitting, pairs of samples (safe samples and failure samples) instead of limit state samples can also be used. It is reported by Jiang et al. (2017) that the safe sample and failure sample can be generated by the safety load F_{l-1} and the failure load F_l calculated with Eq. (7) for each pair of samples, respectively, where ω is a precision parameter and usually $\omega = 0.05$

$$F_{l-1} = (1-\omega)F_{\lim} \tag{7a}$$

$$F_l = (1+\omega)F_{\lim} \tag{7b}$$

Reliability Calculation Steps

Using the limit state samples or sample pairs, the reliability can be calculated with the multiple response surface techniques by the following steps:

1. With the given random variables, select a suitable uniform table to generate initial uniform samples. Use Eq. (2) to obtain the initial uniform samples in the standard norm space.
2. Combine Eqs. (3) and (4) with structural failure analysis techniques to obtain the corresponding limit state samples in the standard normal space.
3. Use the initial limit state samples (or sample pairs) to divide the whole space into s subspaces, and obtain s response surfaces. The principle of subspace division is to ensure that the function fitting with the samples (or sample pairs) in each subspace is achieved with zero residual (or with correct classification).

4. Use the conventional reliability method (e.g., the first-order reliability method) to solve the checking points for the obtained response surfaces. The function call (e.g., finite-element analysis) is executed to check whether the obtained checking points are on the limit state surface. If they are not on the limit state surface, then s limit state samples (or sample pairs) are generated based on the ways listed in Step 2, and added to the current set of samples for iterative calculations. If they are on the limit state surface, the iteration converges.
5. Using the converged multiple response surfaces, the structural reliability can be calculated with Monte Carlo simulation. The failure probability and reliability index are given by Eqs. (8) and (9)

$$\bar{p}_f = \frac{1}{N}\sum_{i=1}^{N} I[G(\bar{X})_i] \tag{8}$$

$$\beta = -\Phi(p_f) \tag{9}$$

where if $G(\bar{X})_i < 0$, $I[G(\bar{X})_i] = 1$; and if $G(\bar{X})_i > 0$, $I[G(\bar{X})_i] = 0$.

Numerical Verification Analysis

Consider the following limit state equation reported by Hadidi et al. (2017):

$$G(u) = 2 - u_2 - 0.1u_1^2 + 0.06u_1^3 \tag{10}$$

where u_1 and u_2 = standard normal random variables.

First, a uniform sample design is carried out for this example with two random variables. A uniform table with eight training samples (N1–N8) is selected and shown in Table 7. According to Eq. (2) with $\lambda = 3$, the initial uniform samples are transformed into those in the standard normal space, as shown in Table 8.

Next, the limit state sample points are solved. Assume u_1 and u_2 as the resistance variable and load variable, respectively. With the given limit state equation Eq. (10) and values of u_1 in Table 8, the assumed limit load values of u_2 are calculated and the corresponding limit state samples are obtained, as shown in Table 9.

Then the whole space is divided into two subspaces with Eq. (5) by using the eight limit state samples in Table 9, and two response surfaces are obtained with Eq. (6) in subspaces. The corresponding checkpoint is solved for each obtained response surface with the first-order reliability method. It is found that the two checkpoints are not on the limit state surface by calling the limit state function, and two limit state samples are obtained by combining the ultimate load values of u_1 with resistance values of u_2 corresponding to these two checkpoints. Add these two limit state samples to update the current total sample points for iterations of response surface fitting. Finally, the fitting is converged after four iterations, and 16 limit state sample points are obtained. The whole space is divided into four subspaces, and there are four limit state samples in each subspace for zero residual fitting, and four response surfaces (RS1–RS4) are also obtained. Because the limit sate samples are used, which satisfy that performance function equals zero, the coefficient a is assumed as $a = 1.0$. The other coefficients of each converged response surface are given in Table 10. Using these coefficients, the response surface equation can be expressed explicitly in each subspace. The obtained response surfaces are drawn and compared with the real limit state surface, as shown in Fig. 10.

From Fig. 10, it can be seen that the fitted failure equation approximates the real limit state equation quite closely in each subspace. Moreover, with the fitted response surface equation, the reliability results are calculated by Monte Carlo simulation, as shown in Table 11. From the comparison of reliability results, it can be seen that the proposed method has a better accuracy and efficiency in reliability analysis.

Structural Reliability Analysis

Reliability Evaluation Using Multiple Response Surfaces Methodology

For this hybrid roof structure, eight random variables are considered and their statistics, which are given in Zhang (2001), are listed in Table 12. The reliability evaluation of bearing capacity is performed by using the MRSs method. The main steps are as follows.

1. Generation of initial uniform samples: As mentioned previously, there are eight random variables, and a uniform design with 64 levels is considered. The uniform design tables $U64(64^8)$

Table 7. Uniform design for the numerical example

Variable	N1	N2	N3	N4	N5	N6	N7	N8
u_1	2	7	8	3	6	5	1	4
u_2	3	5	7	8	2	4	6	8

Table 10. Fitting coefficients of response surface equation

Fitting coefficients	RS1	RS2	RS3	RS4
b_1	0.978	0.267	0.23	116.31
b_2	−1.49	−1.54	0.52	−21.69
c_1	−0.44	−0.22	0.086	13.93
c_2	−5.94	−6.10	−0.45	−9.72

Table 8. Uniform samples in the standard normal space

Variable	N1	N2	N3	N4	N5	N6	N7	N8
u_1	−2.142	2.142	3.0	−1.285	1.285	0.428	−3.0	−0.428
u_2	−1.285	0.428	2.142	3.0	−2.142	−0.428	1.285	3.0

Table 9. Limit state sample points

Variable	N1	N2	N3	N4	N5	N6	N7	N8
u_1	−2.142	2.142	3.0	−1.285	1.285	0.428	−3.0	−0.428
u_2	0.950	2.131	2.720	1.707	1.962	1.986	−0.520	1.976

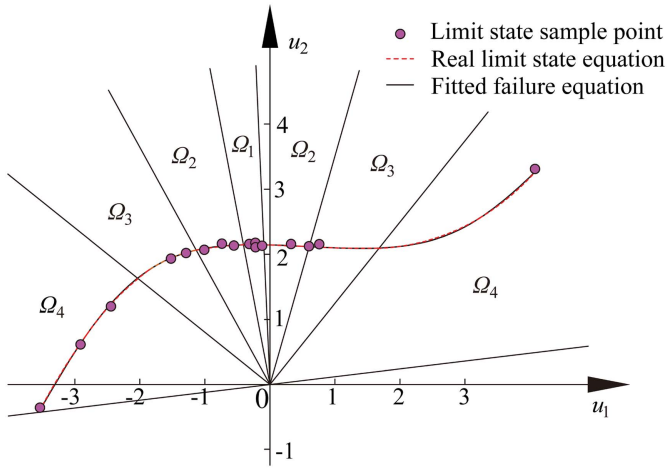

Fig. 10. Comparisons between the fitted failure equation and the real limit state equation.

Table 11. Comparison of reliability calculation results

Method	No. of samples	p_f	β
Proposed method	16	3.43×10^{-3}	1.82
Hadidi et al. (2017)	24	2.17×10^{-3}	2.00
Monte Carlo method	10^6	3.32×10^{-3}	1.82

is selected. Taking $\lambda = 3.0$, the range of variable is obtained as $[-3.0, 3.0]$ with Eq. (2) for each initial sample point in the standard normal space. The initial samples in the Y-space are determined by Eq. (3).

2. Acquisition of limit load for initial samples: Considering the material and geometric nonlinearity, the ultimate bearing capacity of the two models is analyzed. The load combination is shown in the section "Comparisons of Ultimate Bearing Capacity of Two Models." Through the finite-element simulation using 500 load steps, the deterministic structural failure analysis is performed to solve the limit load corresponding to each initial sample points in the Y-space, as shown in Table 13.
3. Fitting of multiple response surfaces: Based on Eq. (7), 64 groups of initial sample pairs, that is, 128 sample points, are obtained. Then these sample points are transformed into those in the standard normal space with Eq. (4), as shown in Table 14, where the S and F denote the safe sample point and failure sample point corresponding to safe and failure loads, respectively.

Among the sample points, N7S can be determined as the closest sample point to the origin. The inner product coefficients between each sample point vector and the N7S sample point vector are calculated according to Eq. (5). Then the total space is divided into four subspaces based on the inner product coefficients.

Using the multiple response surfaces method, four response surfaces can be obtained in the four subspaces. Then the checking points YSD1, YSD2, YSD3, and YSD4 corresponding to each response surface can also be obtained, as shown in Table 15. Transforming YSD1, YSD2, YSD3, and YSD4 to those in the Y-space, it is found that the four transformed checking points are not on the real limit state surface with finite-element analysis. An iterative calculation is needed for reliability evaluation. Four new sample pairs in the standard normal space are obtained with four such transformed checking points and the limit loads. The initial sample points are updated by adding the new sample pairs, and 68 pairs of sample points, that is, 136 sample points, are obtained to divide the subspace and to perform response surface fitting again.

Table 12. Statistics of random variables

X-space variable	Y-space variable	Actual variables	Distribution	Mean	COV	Reference
x_1	y_1	D_L/D_{Ln}	Normal	1.06	0.074	Zhang (2001)
x_2	y_2	S_L/S_{Ln}	Type I largest	1.14	0.285	Zhang (2001)
x_3	y_3	L_L/L_{Ln}	Type I largest	0.71	0.206	Zhang (2001)
x_4	y_4	f_y/f_{yn}	Normal	1.09	0.070	Zhang (2001)
x_5	y_5	γ_1	Normal	1.00	0.150	Assume
x_6	y_6	γ_2	Normal	1.00	0.200	Assume
x_7	y_7	γ_4	Normal	1.00	0.250	Assume
x_8	y_8	γ_3	Normal	1.00	0.250	Assume

Note: Subscript n means the nominal value.

Table 13. Sample points in Y-space and limit load factor

Sample point	y_1	y_2	y_3	y_4	y_5	y_6	y_7	y_8	F_{lim}
N1	1.19	0.68	1.75	0.98	0.63	0.49	1.54	1.43	2.00
N2	0.97	1.73	1.15	1.27	1.26	1.16	1.33	0.64	2.20
N3	0.84	0.89	1.23	0.94	0.97	0.77	1.03	0.43	2.25
N4	1.15	1.57	1.39	0.90	0.69	1.34	1.29	1.36	1.50
N5	1.02	1.81	0.68	1.05	0.76	0.64	1.13	0.69	1.90
...	...	...	...	...	...	...	...	...	...
N58	0.98	0.57	0.68	1.24	1.02	0.60	1.31	1.68	3.20
N59	1.17	0.31	0.48	1.17	1.34	0.57	1.06	0.99	3.25
N60	1.11	1.70	0.39	0.92	1.08	0.55	1.68	1.13	1.65
N61	1.01	0.84	1.08	1.20	1.21	1.23	0.78	1.54	2.50
N62	1.25	1.44	0.46	1.00	0.56	0.92	0.71	0.73	1.80
N63	0.89	1.76	1.05	1.09	1.33	1.14	1.50	1.47	1.80
N64	1.18	1.49	1.11	1.06	0.99	0.90	1.66	0.30	1.70

Table 14. Sampling points in the standard normal space

Sample point	x_1	x_2	x_3	x_4	x_5	x_6	x_7	x_8
N7S	7.81	3.51	4.99	−2.72	1.15	2.44	0.32	0.04
N7F	8.71	3.64	5.13	−2.72	1.15	2.44	0.32	0.04
N28S	9.59	4.17	4.64	−1.8	−1.15	1.33	0.04	−1.33
N28F	10.56	4.31	4.78	−1.8	−1.15	1.33	0.04	−1.33
...	...	...	...	...	...	...	...	...
N59F	47.90	1.09	4.56	1.06	2.26	−2.16	0.23	−0.04
N59S	45.46	0.94	4.42	1.06	2.26	−2.16	0.23	−0.04
N44F	43.68	3.44	3.72	1.8	−1.89	−1.33	−1.8	1.61
N44S	41.41	3.31	3.59	1.8	−1.89	−1.33	−1.8	1.61

Note: Sample points have been sorted by distance from coordinate origin.

Table 15. Checkpoints and reliability index for first iteration

Checkpoint	x_1	x_2	x_3	x_4	x_5	x_6	x_7	x_8	β
YSD1	0.663	5.208	3.360	−3.340	0.048	−0.009	−0.17	0.049	7.077
YSD2	0.758	5.119	2.764	−3.680	0.060	−0.239	0.45	−0.30	6.953
YSD3	0.375	4.009	2.877	−3.250	0.198	0.230	−0.18	0.049	5.934
YSD4	0.564	3.966	3.547	−3.820	−0.025	−0.050	0.135	0.112	6.570

Note: YSD is expressed as checking point.

Table 16. Checkpoints and reliability index for the last iteration

Checkpoint	x_1	x_2	x_3	x_4	x_5	x_6	x_7	x_8	β
YSD17	0.514	0.373	−0.101	−0.166	−3.387	0.971	5.884	2.107	7.206
YSD18	−0.18	−0.41	0.082	0.055	−3.544	0.819	5.517	2.995	7.271
YSD19	0.053	0.289	0.296	−0.244	−3.368	0.494	4.599	2.744	6.364
YSD20	0.214	0.042	−0.121	0.074	−4.011	0.627	4.070	3.465	6.722

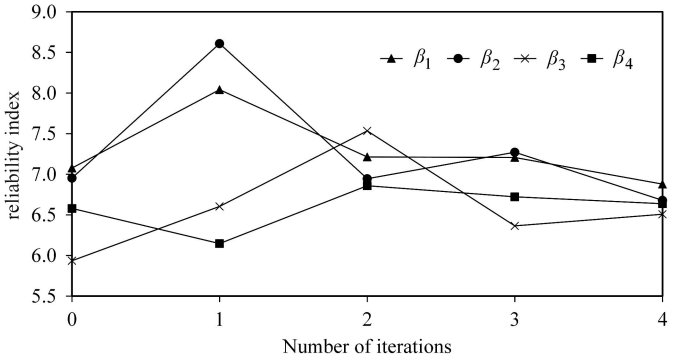

Fig. 11. Iterative calculation of reliability index.

After four iterative steps, the four obtained checking points have been accurately located on the real limit state surface, as shown in Table 16; thus, the iterative fitting stops. A total of 170 sample points including four real checking points are obtained. The reliability indexes of four response surfaces in iteration are shown in Fig. 11.

Summary of Reliability Results

From Table 16, it can be seen that the uncertainties of cable tensions, especially the tensions of the upper suspension cables C_U (corresponding to x_5 variables) and back cables C_W and C_E (corresponding x_7, x_8 variables), which contribute most to reliability index, have stronger impacts on reliability than other uncertainty variables. Thus, special attention should be paid to them in the construction and service periods.

According to the four converged response surfaces and Monte Carlo method, the system failure probability is calculated as $p_f = 6.8996 \times 10^{-12}$, and the corresponding reliability index is 6.76. This indicates that the reliability level of the ultimate bearing capacity is high for the structural model with uncertainties of cable tensions.

Conclusion

This paper proposed a practical model of the uncertainties of cable forces for large hybrid roof structures and studied the influence of the uncertainties on the structure safety. In addition, an advanced multiresponse surface method was studied and applied to reliability evaluation. The main conclusions are as follows:

- The multiple response surfaces method can be well applied to the reliability analysis of both examples with nonlinear failure function and hybrid roof structure with a strong nonlinear mechanical behavior in the loading process. By using this method, the reliability index of the structure considering the uncertainty of cable tensions is calculated as 6.76, which is of a high safety level.
- By multiplying the initial strain of the cable by the uncertain factors, which are determined by errors between the measured and designed cable tensions, the uncertainties of cable tension can be established conveniently in the finite-element model.

- For the hybrid roof structure composed of cables and trusses, the construction deviation will lead to a maximum difference as large as 20.06% between the actual tension of cables and the design tension. The maximum nodal displacement of the structure model without construction deviation is less than that of the structure model with construction deviation under the limit state, and the error is about 15.2%.
- The construction uncertainties of cable tensions have a strong impact on the reliability of the hybrid roof structure, especially the tensions of the upper suspension cables and back cables. Thus, special attention should be paid to them in the construction and service periods.

This study shows that the construction uncertainties in hybrid roof structures do have an impact on structural mechanical performance, especially the stiffness. The positive aspect of this paper is that the proposed multiresponse surface method can realize a reliability evaluation efficiently for such structure with a large number of uncertainties. To summarize, the proposed method in this paper can be widely used in reliability evaluation for large structures with complex mechanical behaviors, which is beneficial to evaluate the reliability for the practical structures.

Data Availability Statement

All data, models, and code generated or used during the study appear in the published article.

Acknowledgments

The research is supported by the National Natural Science Foundation of China (Grant No. 51678072), National Key Research and Development Program of China (2019YFC1511000), and Key Discipline Foundation of Civil Engineering of Changsha University of Science and Technology (18ZDXK01). This support is gratefully acknowledged.

Notation

The following symbols are used in this paper:

a, b_i, c_i = fitting coefficients;
D_w, N_w = diameter and number of cables;
$F_{\lim}$ = ultimate load;
$F^{-1}()$ = inverse function of the cumulative distribution function of variable Y_i;
m = maximum number of variables;
N = number of the sample points;
n = number of experiments;
p_f = failure probability;
q = number of levels of each variable;
T_d, T_m = designed and measured pretensions of each cable;
T_{pre}, T_{post} = cable force values before and after adjusting initial strain;
u_{ij} = element of the selected uniform table;
$U_n(q^m)$ = uniform table;
u_1, u_2 = standard normal random variables;
X_i = variable in standard normal space;
x_{ij} = corresponding element in the standard normal space;
X_0 = closest sample point to the origin among all sample points;
Y_i = a variable in actual space;
β = reliability index;
γ = initial strain factor;
ε = initial strain;
λ = parameter for the possible distribution range of samples;
μ = mean value;
v = cable force errors before and after adjusting initial strain;
ρ_0 = inner product coefficient of X_0 and X_i;
σ = standard deviation;
$\Phi(\cdot)$ = cumulative distribution function of the standard normal variable X_i;
Ω_i = ith subspace; and
ω = precision parameter.

References

Cai, J. G., and J. Feng. 2015. "Form-finding of tensegrity structures using an optimization method." *Eng. Struct.* 104 (Dec): 126–132. https://doi.org/10.1016/j.engstruct.2015.09.028.

Cai, J. G., R. G. Yang, X. Y. Wang, and J. Feng. 2019a. "Effect of initial imperfections of struts on the mechanical behavior of tensegrity structures." *Compos. Struct.* 207 (Jan): 871–876. https://doi.org/10.1016/j.compstruct.2018.09.018.

Cai, J. G., Q. Zhang, J. Feng, and Y. X. Xu. 2019b. "Modeling and kinematic path selection of retractable kirigami roof structures." *Comput.-Aided Civil Infrastruct. Eng.* 34 (4): 352–363. https://doi.org/10.1111/mice.12418.

Cheng, J. 2010. "Determination of cable forces in cable-stayed bridges constructed under parametric uncertainty." *Eng. Comput.* 27 (3): 301–321. https://doi.org/10.1108/02644401011029907.

Cheng, M. 2014. "Probability analysis and parameters identification of cable tested tension by frequency method." [In Chinese.] Master dissertation, School of Transportation Science and Engineering, Harbin Institute of Technology.

Dai, L., H. Bian, L. Wang, and M. Potier-Ferry. 2020. "Prestress loss diagnostics in pretensioned concrete structures with corrosive cracking." *J. Struct. Eng.* 146 (3): 04020013. https://doi.org/10.1061/(ASCE)ST.1943-541X.0002554.

Deng, H., M. R. Zhang, H. C. Liu, S. L. Dong, Z. H. Zhang, and L. Q. Chen. 2016. "Numerical analysis of the pretension deviations of a novel crescent-shaped tensile canopy structural system." *Eng. Struct.* 119 (Jul): 24–33. https://doi.org/10.1016/j.engstruct.2016.04.005.

Deng, H., Y. Z. Zu, J. J. Shen, G. B. Bai, S. L. Dong, Z. H. Zhang, and L. Q. Chen. 2013. "Analysis and experiment on erection process of a crescent-shaped cable-truss canopy structure." [In Chinese.] *J. Zhejiang Univ. (Eng. Sci.)* 47 (3): 488–494. https://doi.org/10.3785/j.issn.1008-973X.2013.03.013.

Dubourg, V., B. Sudret, and F. Deheeger. 2013. "Metamodel -based importance sampling for structural reliability analysis." *Probab. Eng. Mech.* 33 (Jul): 47–57. https://doi.org/10.1016/j.probengmech.2013.02.002.

Fang, K. T. and Y. Wang. 1994. *Number-theoretic methods in statistics*. London: Chapman & Hall.

Feng, F. 2005. "Structural behavior and design methods of Tensegrity domes." *J. Constr. Steel Res.* 61 (1): 23–35. https://doi.org/10.1016/j.jcsr.2004.06.004.

Fuller, B. R. 1975. *Synergetics: Explorations in the geometry of thinking*. New York: Macmillan.

Geiger, D. H., A. Stefaniuk, and D. Chen. 1986. "The design and construction of two cable domes for the Korean Olympics." In Vol. 2 of *Proc., IASS Symp. Osaka, Shells, Membranes and Space Frames*, 265–272. Amsterdam, Netherlands: Elsevier.

Guimarães, H., J. C. Matos, and A. A. Henriques. 2018. "An innovative adaptive sparse response surface method for structural reliability analysis." *Struct. Saf.* 73 (Jul): 12–28. https://doi.org/10.1016/j.strusafe.2018.02.001.

Hadidi, A., B. F. Azar, and A. Rafiee. 2017. "Efficient response surface method for high-dimensional structural reliability analysis." *Struct. Saf.* 68 (Sep): 15–27. https://doi.org/10.1016/j.strusafe.2017.03.006.

Jiang, Y. B., Q. Cao, X. Kong, and G. Y. Liao. 2016. "Stiffness study of inner concave cable–arch structure based on an efficient method." *Adv. Struct. Eng.* 19 (12): 1927–1939. https://doi.org/10.1177/1369433216649394.

Jiang, Y. B., J. Luo, G. Y. Liao, Y. L. Zhao, and J. R. Zhang. 2015. "An efficient method for generation of uniform support vector and its application in structural failure function fitting." *Struct. Saf.* 54 (May): 1–9. https://doi.org/10.1016/j.strusafe.2014.12.004.

Jiang, Y. B., L. J. Zhao, M. Beer, E. Patelli, M. Broggi, J. Luo, Y. H. He, and J. R. Zhang. 2017. "Multiple response surfaces method with advanced classification of samples for structural failure function fitting." *Struct. Saf.* 64 (Jan): 87–97. https://doi.org/10.1016/j.strusafe.2016.10.002.

Ju, S., R. A. Shenoi, D. Jiang, and A. J. Sobey. 2013. "Multi-parameter optimization of lightweight composite triangular truss structure based on response surface methodology." *Compos. Struct.* 97 (2): 107–116. https://doi.org/10.1016/j.compstruct.2012.10.025.

Juan, S. H., and J. M. M. Tur. 2008. "Tensegrity frameworks: Static analysis review." *Mech. Mach. Theory* 43 (7): 859–881. https://doi.org/10.1016/j.mechmachtheory.2007.06.010.

Kebiche, K., M. N. Kazi, and R. Motro. 1999. "Geometrical non-linear analysis of tensegrity systems." *Eng. Struct.* 21 (9): 864–876. https://doi.org/10.1016/S0141-0296(98)00014-5.

Kmet, S., and M. Mojdis. 2013. "Time-dependent analysis of cable domes using a modified dynamic relaxation method and creep theory." *Comput. Struct.* 125 (1): 11–22. https://doi.org/10.1016/j.compstruc.2013.04.019.

Kmet, S., M. Tomko, and J. Brda. 2007. "Time-dependent analysis and simulation-based reliability assessment of suspended cables with rheological properties." *Adv. Eng. Software* 38 (8–9): 561–575. https://doi.org/10.1016/j.advengsoft.2006.08.022.

Marelli, S., and B. Sudret. 2018. "An active-learning algorithm that combines sparse polynomial chaos expansions and bootstrap for structural reliability analysis." *Struct. Saf.* 75 (Nov): 67–74. https://doi.org/10.1016/j.strusafe.2018.06.003.

MOHURD (Ministry of Housing and Urban-Rural Development of the People's Republic of China). 2012. *Load code for the design of building structures*. [In Chinese.] GB50009-2012. Beijing: China Building Industry Press.

Morino, S. 1998. "Recent developments in hybrid structures in Japan—Research, design and construction." *Eng. Struct.* 20 (4–6): 336–346. https://doi.org/10.1016/S0141-0296(97)00022-9.

Papadopoulos, V., D. G. Giovanis, N. D. Lagaros, and M. Papadrakakis. 2012. "Accelerated subset simulation with neural networks for reliability analysis." *Comput. Meth. Appl. Mech. Eng.* 223–224 (Jun): 70–80. https://doi.org/10.1016/j.cma.2012.02.013.

Phocas, M. C., and K. Alexandrou. 2018. "Numerical analysis and cable activation in hybrid bending-active structures with multiple cables." *Eng. Struct.* 174 (Nov): 561–572. https://doi.org/10.1016/j.engstruct.2018.07.089.

Rosenblatt, M. 1952. "Remarks on a multivariate transformation." *Ann. Math. Stat.* 23 (3): 470–472. https://doi.org/10.1214/aoms/1177729394.

Schobi, R., B. Sudret, and J. Wiart. 2015. "Polynomial-chaos-based kriging." *Int. J. Uncertainty Quantif.* 5 (2): 171–193. https://doi.org/10.1615/Int.J.UncertaintyQuantification.2015012467.

Sultan, C., M. Corless, and R. E. Skelton. 2001. "The prestressability problem of tensegrity structures: Some analytical solutions." *Int. J. Solids Struct.* 38 (30): 5223–5252. https://doi.org/10.1016/S0020-7683(00)00401-7.

Sultan, C., M. Corless, and R. E. Skelton. 2002. "Linear dynamics of tensegrity structures." *Eng. Struct.* 24 (6): 671–685. https://doi.org/10.1016/S0141-0296(01)00130-4.

Teixeira, R., N. María, and A. O'Connor. 2020. "Adaptive approaches in metamodel-based reliability analysis: A review." *Struct. Saf.* 89 (2021): 102019. https://doi.org/10.1016/j.strusafe.2020.102019.

Tibert, G., and S. Pellegrino. 2003. "Review of form-finding methods for tensegrity structures." *Int. J. Space Struct.* 18 (4): 209–223. https://doi.org/10.1260/026635103322987940.

Wakefield, D. S. 1999. "Engineering analysis of tension structures: Theory and practice." *Eng. Struct.* 21 (8): 680–690. https://doi.org/10.1016/S0141-0296(98)00023-6.

Wang, L., L. Z. Dai, H. B. Bian, and Y. F. Ma. 2019. "Concrete cracking prediction under combined prestress and strand corrosion." *Struct. Infrastruct. Eng.* 15 (3): 285–295. https://doi.org/10.1080/15732479.2018.1550519.

Wang, Z. Y., and A. Shafieezadeh. 2019. "REAK: Reliability analysis through error rate-based adaptive kriging." *Reliab. Eng. Syst. Saf.* 182 (Feb): 33–45. https://doi.org/10.1016/j.ress.2018.10.004.

Williamson, D., R. E. Skelton, and J. Han. 2003. "Equilibrium conditions of a tensegrity structure." *Int. J. Solids Struct.* 40 (23): 6347–6367. https://doi.org/10.1016/S0020-7683(03)00400-1.

Xiao, N. C., H. Y. Zhan, and K. Yuan. 2020. "A new reliability method for small failure probability problems by combining the adaptive importance sampling and surrogate models." *Comput. Meth. Appl. Mech. Eng.* 372 (Dec): 113336. https://doi.org/10.1016/j.cma.2020.113336.

Xue, G. F., H. Z. Dai, H. Zhang, and W. Wang. 2017. "A new unbiased metamodel method for efficient reliability analysis." *Struct. Saf.* 67 (Jul): 1–10. https://doi.org/10.1016/j.strusafe.2017.03.005.

Yan, X. Y., Y. Yang, Z. H. Chen, and Q. Ma. 2019. "Mechanical properties of a hybrid cable dome under non-uniform snow distribution." *J. Constr. Steel Res.* 153 (Feb): 519–532. https://doi.org/10.1016/j.jcsr.2018.10.022.

Yasuhiko, H. G., and M. Wu. 1999. "Analytical method of structural behaviors of a hybrid structure consisting of cables and rigid structures." *Eng. Struct.* 21 (8): 726–736. https://doi.org/10.1016/S0141-0296(98)00027-3.

Zhang, J. Y., and M. Ohsaki. 2006. "Adaptive force density method for form-finding problem of tensegrity structures." *Int. J. Solids Struct.* 43 (18): 5658–5673. https://doi.org/10.1016/j.ijsolstr.2005.10.011.

Zhang, Q., N. Pan, M. Meloni, D. Lu, J. G. Cai, and J. Feng. 2020. "Reliability analysis of radially retractable roofs with revolute joint clearances." *Reliab. Eng. Syst. Saf.* 208 (2021): 107401. https://doi.org/10.1016/j.ress.2020.107401.

Zhang, X. P. 2001. *Reliability analysis and design for building structures*. [In Chinese.] Beijing: Science Press.